JOURNAL OF MATERIALS SCIENCE **40** (2005) 5867–5873

Mechanical properties of bread crumbs from tomography based Finite Element simulations

P. BABIN*
GPM2, INP Grenoble, BP 46, 38402 Saint Martin d'Hères cedex; Science Computers Consultants, 8, rue de la Richelandière, Parc Giron, 42100 St Etienne
E-mail: perrine.babin@gpm2.inpg.fr

G. DELLA VALLE
URPOI, INRA BP 71627, 44316 Nantes Cedex 3

R. DENDIEVEL
GPM2, INP Grenoble, BP 46, 38402 Saint Martin d'Hères cedex

N. LASSOUED
URPOI, INRA BP 71627, 44316 Nantes Cedex 3; UMR INRA-ENSIA, Food Science Department, 1 av des Olympiades, 91744 Massy Cedex; CTCPA, rue Marcel Luquet, 32000 Auch

L. SALVO
GPM2, INP Grenoble, BP 46, 38402 Saint Martin d'Hères cedex

Finite Element analyses of cellular cereal products were performed in order to link microstructure and mechanical properties. Different samples of model breads were elaborated by modifying the composition in order to generate different microstructures. Their final 3D cellular structure was investigated by X-ray tomography to provide an accurate description of microstructural characteristics. Moreover, an *in-situ* study of the fermentation step was performed to assess the bubble structure development in the dough. Two different approaches of modelling were explored in order to take into account accurately microstructural features: 3D finite cubic element mesh based on a direct transcription of the voxel image and a tetrahedral mesh. The predicted Young's modulus values were found in good agreement with experimental ones. Mechanical modelling of the fermentation step was then performed with tetrahedral meshes. At the end of the fermentation, when products have reached a relative density of about 0.3, the mechanical properties differ, allowing discriminating the different microstructures.

1. Introduction

The consumer appreciation of solid food foams like bread, extruded cereals, biscuits and cakes is strongly linked to the texture. The control of the sensory properties of such products, which is still a challenge, requires a better understanding of relationships between composition, cellular structure formation mechanisms and final texture. For texture, sensory properties of solid food foams are well known to be related to both mechanical properties and cellular structure [1, 2]. In this context, determining the relationships between a given mechanical property and the cellular structure is thus of prime importance. Since cellular cereal products can be considered, from morphological and topological points of view, like metallic or polymeric foams, it is tempting to address this problem by referring to Gibson & Ashby's model [3]. Such scaling laws are shown to be efficient to assess the effect of the relative density on mechanical properties like Young's modulus or strength of extruded starchy materials [4, 5] or bread [6, 7]. However, for the same density, mechanical properties and sensory properties are also sensitive to microstructural dispersions [6–9]. The purpose of this work is to develop an approach which focuses on such microstructural effects, from both imaging and mechanical points of view.

*Author to whom all correspondence should be addressed.
0022-2461
DOI: 10.1007/s10853-005-5021-x

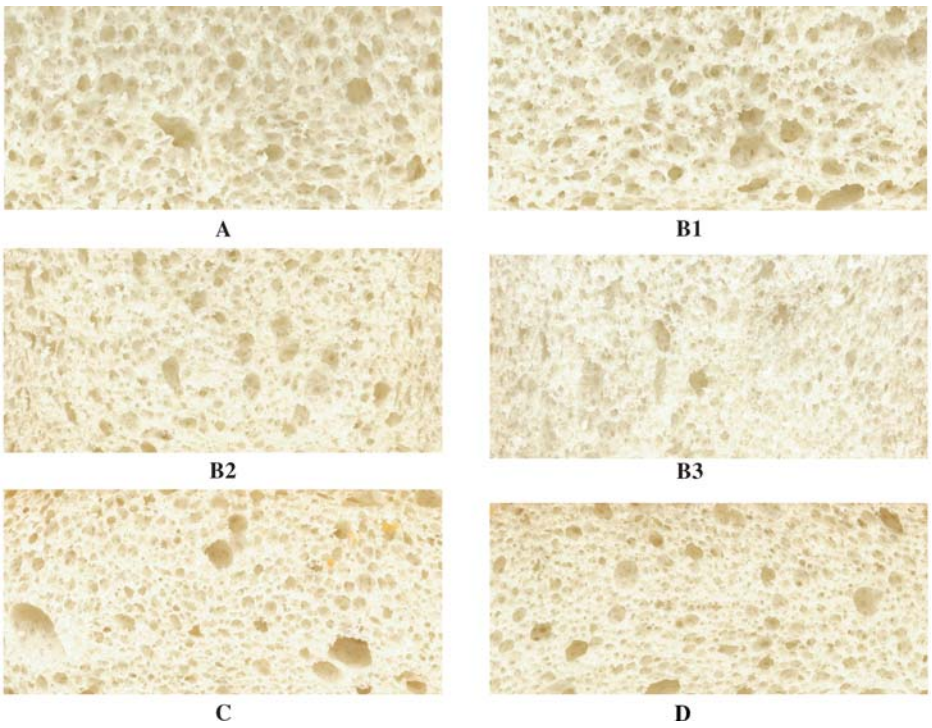

Figure 1 Scanned images of the crumb texture of the baked products A, B, C and D.

Generally, scanner [10], video image [11] or Magnetic Resonance Imaging [12, 13] techniques are used to capture the microstructure of cellular food products. Quantification is possible but only at a macroscopic scale and for global structural features such as density or mean cell size, assuming that methodological uncertainties due to image analysis are solved. Moreover, these techniques give only 2D information which limits the interpretation of the results, especially in the case of such complex architectures. For the last years, X-ray tomography has been proved particularly well-suited for the 3D investigation of cellular materials [14]. Very recently, it has also been applied to cellular food products [9, 15, 16] but without quantification. These studies have shown that tomography images allow describing accurately in three dimensions the complexity of the morphology of cellular food products. In addition, this technique enables dynamic studies. We present in this paper the application of a newly developed X-ray "fast" tomography technique to the *in situ* following of cellular food fermentation.

From a mechanical point of view, structure-property relationships of heterogeneous materials are often addressed through theories incorporating more or less realistic microstructural information [17]. They are however difficult to apply to the case of cellular complex architectures [18]. To deal directly with the 3D images is a tempting way to overcome such difficulties. In our case, their conversion to input data is performed through two techniques: a straightforward "voxel to element" transcription or a tetrahedral mesh constructed on the "smoothed" volume [19–21].

In this study, different bread crumbs leading to distinct cellular structures are investigated. An *in-situ* study by tomography is performed to characterize not only the final cellular structure, but also to follow the whole process of development of microstructure during fermentation stage. Different compositions are studied in order to understand how and when the microstructural dispersions appear and develop. Two Finite Element approaches are performed on the tomography images of the final products and the results are compared to experimental compression test data. Finally, numerical simulations are applied on images extracted at different stages of the fermentation process.

2. Materials and methods

2.1. Cellular cereal products

Bread crumbs with various compositions (flour, water, sucrose, salt, oil and yeast), as reported in Table I, were chosen for this study.

B1, B2 and B3 refer to products moulded differently in order to get different microstructures with exactly the same composition. A, B, C and D specimens were dedicated to the study of the cellular microstructures of baked products. They exhibit rather different microstructures (see Fig. 1). For the *in-situ* study of fermentation, only compositions A and B were kept because high sucrose content of C and D delayed the beginning of the fermentation. Three additional compositions were studied and among them the French bread

TABLE I Composition of specimens of bread crumbs tested. Contents are given in % of 100 g of flour

	Water	Sucrose	Oil	Yeast	Salt
A	60	2	2		
B1, B2, B3	55	2	10		
C	65	10	10	3	2
D	55	15	2		
E	65	2	2		
F	62	0	0	2.5	2.2
G	60	2	2	1.5	2

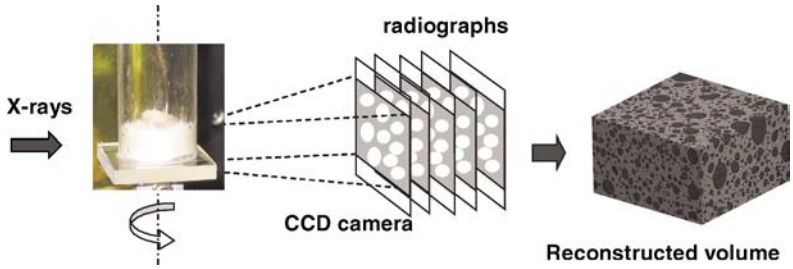

Figure 2 Schematic view of the experimental set-up and principle of X-ray tomography.

(F). By comparison with composition (A), we chose to characterize also compositions to test the specific effects of water (E) and yeast content (G). The reduction of yeast content is expected to reduce the kinetic of fermentation.

The wheat flour was standard commercial bread flour (provided by Grands Moulins de Paris, F-92 Gennevilliers). It was mixed with yeast and water, previously blended with sucrose and salt. Oil was finally added to the mix. The dough was placed in a cylindrical glass mould to rest in a proofing room at 25°C for 90 min (fermentation stage) and was finally baked during one hour at 180°C. More details about the breadmaking process are given elsewhere [22]. Each product was divided in two parts. The first half was used for the compression tests and the other one for the characterization of the final cellular structure by tomography. Concerning the *in-situ* study of fermentation by tomography, a few milligrams specimens were taken from the dough just after kneading.

2.2. Experimental compression tests

Cylindrical specimens (30 mm high and 50 mm diameter) were tested in compression between parallel plates on an Instron universal testing machine. A cross head speed of 50 mm/min was used. Experimental Young's moduli were obtained for baked products A, B, C and D. Repetitions of the experiments lead to an experimental incertitude of $\pm 15\%$, mainly due to the heterogeneity of bread structure, which is reduced for compositions including fat. The tests have been pursued until the complete densification of the sample in order to assess the constitutive material properties. The Young's moduli E_s measured in this last stage were found quite similar for all the compositions. Different values of intrinsic modulus could be expected from these differences of composition. For instance, the larger content of moisture, sugar and fat of composition C is expected to plastify the matrix and thus lead to lower values of E_s. In spite of this uncertainty, the same value of $E_s = 0.63$ MPa was used in all the numerical simulations and the significance of this hypothesis has to be checked further.

2.3. X-ray tomography

The general principle of X-ray tomography is now widely referenced in the literature [23]. We just recall the specific conditions used for the present study. It was carried out at ESRF (European Synchrotron Radiation Facility, Grenoble, F-38). The use of synchrotron radiation allows to obtain very good quality images in terms of signal-to-noise ratio and a high spatial resolution. Specimens A, B, C and D, extracted from final loaves of bread, were scanned on beamline ID19 with a resolution of 10 microns. Resulting 3D data are 256 grey level images of $700 \times 700 \times 700$ voxels.

The *in-situ* study of the fermentation step was achieved on beamline BM05, using a specifically designed "fast" tomography technique. Exposure time of a single radiograph of 20 milliseconds, allowed a scan of 400 radios over 180° degrees within less than 30 s. Product changes during this interval could be reasonably discarded in comparison with its overall evolution during total fermentation time. Dough specimens of a few milligrams were initially taken and put into® Plexiglas cylinders of 7 mm diameter (Fig. 2). The vertical field of view was about 4 mm high and remained fixed (Eulerian point of view). Scans were recorded every 5 or 10 minutes (depending on the yeast content), to get a real "movie" of the whole process. All specimens were proofed during two hours at a constant temperature of 25°C, except for the specimen G with 1.5% yeast, which was followed during three hours. The fermentation was made longer than usual to observe the coalescence mechanisms until very low densities. The spatial resolution was 15 μm. The corresponding Region of Interest (ROI) was in this case $440 \times 440 \times 256$ voxels (i.e. $6.6 \times 6.6 \times 3.8$ mm^3).

2.4. Finite element simulation

As explained in the introduction, the digital 3D images obtained are the starting point of the Finite Element (FE) simulations. Attention is paid on the Young's modulus of the specimens. Boundary conditions corresponding to a uniaxial compression test are applied and isotropic linear elastic constitutive material characteristics are assumed. As explained previously, the constitutive Young's modulus has been identified as the slope of the experimental compression curve at the end of the densification stage. No significant differences being found for the various compositions, the same value of 0.63 MPa was used for all the calculations. A Poisson's ratio of 0.3 was used. Two different approaches were performed to produce FE meshes reflecting the actual bread cellular microstructure.

The first one consists in a straightforward conversion of the voxel structure of the 3D digital images. Each voxel becomes an eight node hexahedral element. Only the voxels belonging to the cell walls, to say, with a grey

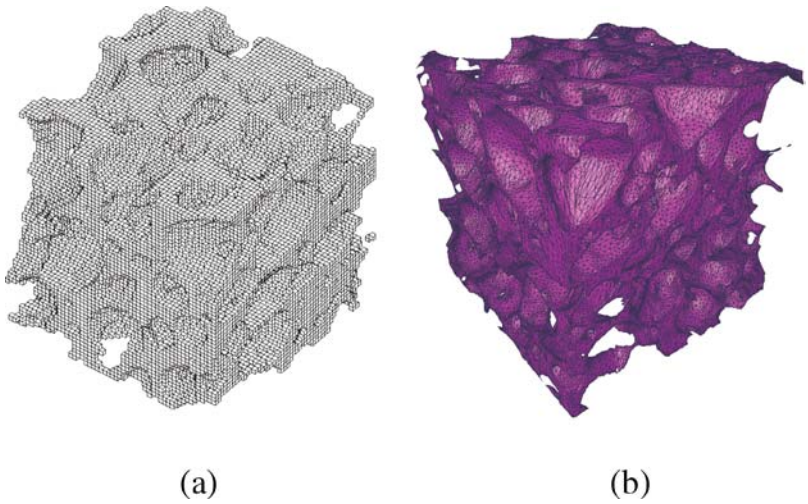

Figure 3 Illustration of the two different meshes: hexahedral (a) or tetrahedral (b) elements.

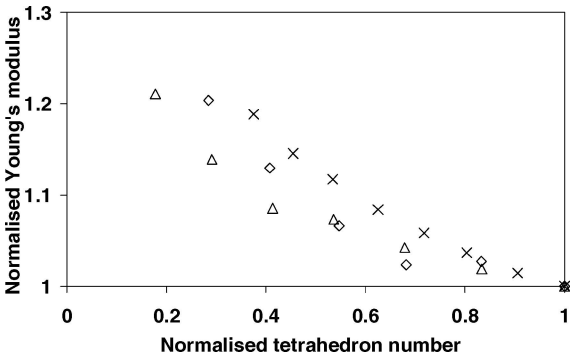

Figure 4 Influence of the number of tetrahedral element on the Young's modulus. ○: sample A, ◇: sample B3 and × : sample C. Number of elements are normalised by the maximum number tested. Young's modulus is normalised in consequence.

level beyond a specified threshold value, are considered (Fig. 3a). As detailed in next section, specimens A to D exhibit relative densities ranging from 0.18 to 0.34. For a volume of $700 \times 700 \times 700$ voxels, it leads to a number of elements completely out of the memory capacity of standard computers. Sub-resolution technique is a solution to overcome this limitation. It consists in replacing a group of eight voxels by only one voxel, the grey level of which being the average of the eight grey level values. Such a procedure can be repeated. Each sub-resolution leads to a loss of information about the morphology of the microstructure. A compromise has to be found between the number of elements and the coarseness of the description. In the present case, three successive sub-resolution operations were systematically performed.

The second approach consists in a preliminary transformation of the voxel structure based on the marching cubes algorithm [24]. The obtained smoothed surfaces are then discretised in triangular elements. Finally, a volumic tetrahedral mesh is built from this triangular discretisation. The microstructure appears more realistic than the initial "voxelised" image (Fig. 3b). Moreover, it is possible to control the fineness of the triangular mesh of the surface and consequently the fineness of the 3D mesh. The influence of the number of elements was studied in the case of this second approach. Results are presented in Fig. 4 for three different samples. Once the values have been normalised to take into account the density dependency, it is found that the effective Young's modulus decreases when the number of element increases until reaching a constant value. The largest numbers of elements used here range from 4.10^5 to 3.10^5 for specimens A, B and C. Such tests were performed systematically for all the specimens. In the following, numerical values presented correspond always to such numbers of elements, above which no significant effect on the Young's modulus is detected.

3. Results and discussion

3.1. Mechanical properties of bread crumb

On Table II are displayed the experimental results concerning the baked products. For relative densities ranging from 0.18 to 0.34, Young's modulus increases from about 29 to 94 kPa. Although having the same composition, B1, B2 and B3 products present different moduli, which may be due to the different way of moulding : B1 was baked in an open mould whereas, B2 and B3 were baked in a closed one, which limited bread oven rise during baking and modified the density of the baked products. For C and D products, the high content in sucrose causes an increase in final product density.

Numerical calculations were performed on volumes issued from X-ray tomography, the relative densities of which were taken exactly the same as the experimental ones by adjusting adequately the threshold in grey level. The results are given on Fig. 5 for the two

TABLE II Experimental results for the baked products (specimens A to D)

Baked products	A	B1	B2	B3	C	D
[a]Density ($\rho*$), g/cm^3	0.21	0.24	0.26	0.26	0.33	0.4
[b]Relative density ($\rho*/\rho_s$)	0.18	0.20	0.22	0.22	0.28	0.34
Young's modulus, Pa (± 15%)	28630	40780	41500	41600	54260	93730

[a] ρ^* is measured by rapeseed displacement.
[b] ρ_s is deduced from concentrations of each ingredient by a simple additive rule.

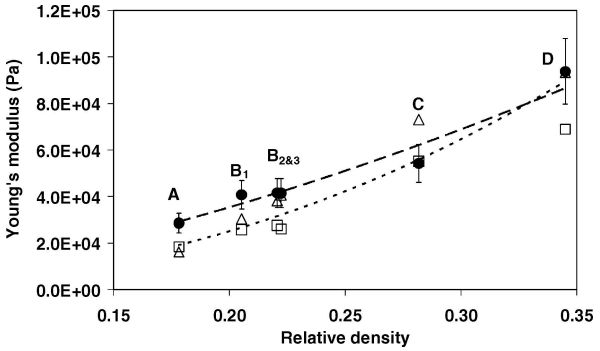

Figure 5 Evolution of the Young's Modulus in function of relative density for the baked cereal products. • : experimental moduli, □ : numerical moduli obtained with a hexahedral mesh and △: numerical moduli obtained with a tetrahedral mesh.

methods detailed in Section 2.4. Experimental results are also reported. Experimental and numerical values are in quite good agreement although constitutive E_s value was not adjusted but experimentally determined. Even if the Finite Element volumes are rather small (4 mm^3) in comparison with experimental ones, they are assumed to contain enough microstructural characteristics in order to be mechanically representative. This hypothesis has to be checked by performing systematic study of the influence of their size on the Young's modulus.

Both experimental and numerical results were fitted by a power law leading respectively to the following relationship between effective Young's modulus and relative density

$$\left(\frac{E^*}{E_s}\right)_{\text{exp.}} \propto \left(\frac{\rho^*}{\rho_s}\right)^{1.6} \qquad \left(\frac{E^*}{E_s}\right)_{\text{FEM}} \propto \left(\frac{\rho^*}{\rho_s}\right)^{2.3}$$

with a good accuracy (correlation coefficient $R^2 \geq 0.9$). According to the Gibson and Ashby's work, such exponent values suggest that these bread crumbs are closer to an open-cell foam ($n = 2$) than a closed-cell foam ($n = 1$). The higher value ($n = 2.3$) of the numerical fit may be due to the image treatments, which can thicken or disconnect some cell walls. Moreover, at low relative densities (<0.25), such thickening or removing effects lead to predicted values systematically lower than experimental ones.

The comparison between the two simulation methods shows that hexahedral elements lead to a systematically lower modulus and the discrepancy between hexahedral and tetrahedral elements increases with the relative density. Apart from sample C, which, as stated before, has likely a lower E_s value, tetrahedral meshing would yield a better agreement, which underlines its relevance for taking the microstructure into account. That is why only this method is used in the following.

3.2. Mechanical discrimination during fermentation

On Fig. 6 is displayed the evolution of the microstructure during the fermentation stage of sample E. For sake of clarity, only five 2D pictures, among the overall twenty-five recorded, are shown.

From a qualitative point of view, two regimes can be distinguished. At the beginning of the fermentation stage, small spherical bubbles are observed. Production of CO_2 leads to the isotropic growth of these spherical cells until about 50 min. After this time, bubbles keep on with growing and deforming each other. The film matrix separating two bubbles is extended until rupture: the coalescence phenomenon leads to complex cavity shapes.

From a macroscopic quantitative point of view, relative densities measured from image analysis and their evolution, are represented in Fig. 7 for the five compositions A, B, E, F and G. For sample G, the smaller content of yeast explains the lower kinetics of density decrease, likely due to slower CO_2 production. The transition between the two regimes is highlighted on the graph by the change of curvature.

When considering different fermentation times, Fig. 7 suggests the existence of different microstructures for the same values of relative density (horizontal dashed lines), from which different mechanical behaviours may be expected. Baking involves dough to

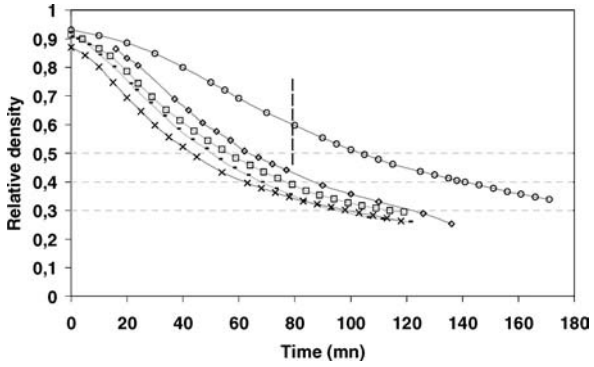

Figure 7 Evolution of the relative density during fermentation of the five different samples: - sample *A*, ◇ sample *B1*, × sample *E*, □ sample *F* and ○ sample *G*. Transition between growth and coalescence regimes is highlighted for specimen *G*.

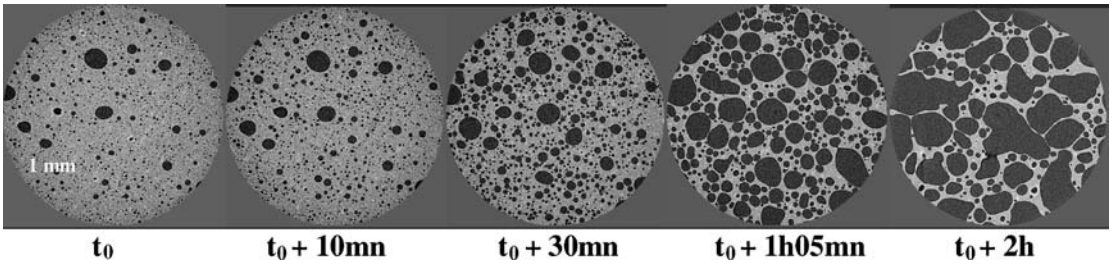

Figure 6 Evolution of the microstructure during the fermentation stage of sample *E*.

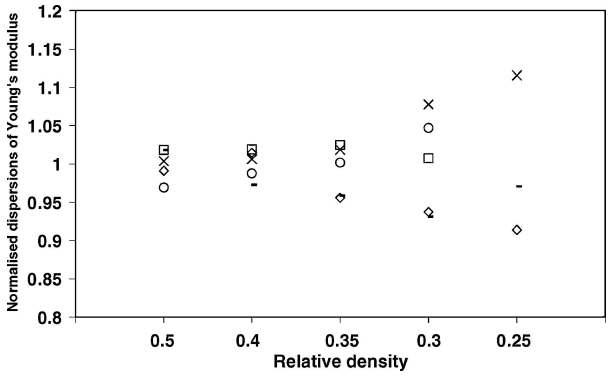

Figure 8 Dispersion of the numerical Young's moduli in function of the relative density of five samples during the fermentation process: - sample *A*, ◇ sample *B1*, × sample *E*, □ sample *F* and ○ sample *G*.

crumb transition which induces important biochemical changes and this stage cannot fully be discarded. However, it has been shown that the main cellular characteristics features generated during fermentation are still present after baking, and discriminate crumbs made from dough processed differently or from different compositions [13, 25]. Therefore, for each composition, Finite Element calculations have been performed on microstructures taken at selected relative densities from 0.5 to 0.25, assuming that they depict the crumb with its intrinsic mechanical properties. In this purpose, tetrahedral meshing method was used, owing to the preceding discussed performances. Results are shown on Fig. 8. Results have been normalised: for each relative density, the value corresponding to unity is the average of the different specimens.

For higher densities, all the compositions lead to close predictions of their mechanical properties. Significant dispersions appear for relative densities lower than 0.35. This suggests that microstructures resulting from different compositions can be discriminated at the end of the fermentation process, at least from a mechanical point of view, which is in agreement with the results of Van Vliet [26]: above a void volumic fraction of 0.7, bubbles undergo a steric constraint and deform each other strongly. Moreover, such results give us a tendency for each composition to generate "soft" or "hard" products, for the same relative density, which is beyond the actual capacity of mechanical tests, because of experimental limits. It is also of practical consequence from a sensorial point of view. Further progress in this study will be to determine the relevant differences between the microstructures in terms of cellular distribution, which is addressed by the 3D analysis of tomography images.

Such results suggest a possible way to monitor the process to modify product composition or processing in order to change its microstructure and, consequently, the expected mechanical properties.

4. Conclusion

By studying products with different compositions, according to 3D imaging and mechanical points of view, we have developed an approach which ascertains the microstructural effects of bread crumbs considered as solid foams. Experimental testing suggested that intrinsic modulus does not depend on composition. A good fit to classical Gibson & Ashby's model for open cell foams was obtained. X-ray tomography has been shown particularly relevant to generate realistic numerical microstructures, and especially during *in-situ* fermentation experiments for the design of different microstructures for same relative density of the crumbs. Numerical simulation was achieved, assuming linear elastic behaviour of the constitutive material, and by emphasizing the meshing method, tetrahedral scheme was selected, due to good agreement with experimental results of mechanical properties. By applying this numerical simulation to virtual crumbs, a threshold value of relative density was determined beyond which the effects of microstructure could be discriminated. This approach can be improved in different ways: testing the sensitivity to the compositions of the intrinsic material properties including the accurate determination of this property and determining the main microstructural features to take into account for the computation of mechanical properties, are two prospects currently being addressed.

Acknowledgment

This work has been carried out in the frame of CANAL-Salve program from the French Ministry of Research within which partners' contribution is gratefully acknowledged. The teams of beam lines BM05 and ID19 at ESRF are also deeply acknowledged. The authors acknowledge H. Chiron for his excellent technical assistance. They are also grateful to Science Computers Consultant (SCC F42-St Etienne) for financial support of this study, and especially Ch. David for helpful discussion.

References

1. G. E. ATTENBURROW, R. M. GOODBAND, L. J. TAYLOR and P. J. LILLFORD, *J. Cereal Sci.* **9** (1989) 61.
2. E. J. PYLER, in "Baking Science and Technology" (Elsevier, London, 1988) Vol. 2 p. 850.
3. L. J. GIBSON and M. F. ASHBY, "Cellular Solids" (Cambridge University Press, Cambridge, UK, 1997).
4. S. C. WARBURTON, A. M. DONALD and A. C. SMITH, *J. Mat. Sci.* **25** (1990) 4001.
5. D. LOURDIN, G. DELLA VALLE and P. COLONNA, *Carbohyd. Polym.* **27** (1995) 261.
6. C. J. A. M. KEETELS, T. VAN VLIET and P. WALSTRA, *J. Cereal Sci.* **24** (1996) 27.
7. M. C. ZGHAL, M. G. SCANLON and H. G. SAPIRSTEIN, *J. Cereal Sci.* **36** (2002) 167.
8. M. G. SCANLON and M. C. ZGHAL, *Food Res. Inter.* **34** (2001) 841.
9. P. BABIN, G. DELLA VALLE, R. DENDIEVEL and L. SALVO, in Proceedings of the 5th International Conference Engineering and Food (Montpellier France, 2004).
10. D. E. ROGERS, D. D. DAY and M. C. OLEWNICK, *Cereal Foods World* **40** (1995) 498.
11. H. D. SAPIRSTEIN, R. ROLLER and W. BUSHUK, *Cereal Chem.* **71** (1994) 383.
12. H. TAKANO, N. ISHIDA, M. KOIZUMI and H. KANO, *J. Food Sci.* **67** (2002) 244.
13. J. P. M. VAN DUYNHOVEN, G. M. P. VAN KEMPEN, R. VAN SLUIS, B. RIEGER, P. WEEGELS, L. J. VAN VLIET and K. NICOLAY, *Cereal Chem.* **80** (2003) 390.
14. A. ELMOUTAOUAKKIL, L. SALVO, E. MAIRE and G. PEIX, *Adv. Eng. Mater.* **4** (2002) 803.

15. P. M. FALCONE, A. BAIANO, F. ZANINI, L. MANCINI, G. TROMBA, F. MONTANARI and M. A. DEL NOBILE, *J. Food Science* **69** (2004) 38.
16. K. S. LIM and M. BARIGOU, in Proceedings of the 5th International Conference Engineering and Food (Montpellier, France, 2004).
17. S. TORQUATO, "Random Heterogeneous Materials: Microstructure and Macroscopic Properties" (Springer Verlag, New-York, 2001).
18. A. P. ROBERTS and E. J. GARBOCZI, *Proc. R. Soc. Lond. A* **458** (2002) 1033.
19. D. ULRICH, B. VAN RIETBERGEN, H. WEINANS and P. RÜEGSEGGER, *J. Biomech.* **31** (1998) 1187.
20. A. P. ROBERTS and E. J. GARBOCZI, *J. Mech. Phys. Solids* **50** (2002) 33.
21. E. MAIRE, A. FAZEKAS, L. SALVO, R. DENDIEVEL, S. YOUSSEF, P. CLOETENS and J. M. LETANG, *Compos. Sci. Technol.* **63** (2003) 2431.
22. N. LASSOUED, G. DELLA VALLE, B. LAUNAY, D. LOURDIN and C. MICHON, in Proceedings of the 5th International Conference Engineering and Food (Montpellier, France, 2004).
23. J. BARUCHEL, J. Y. BUFFIERE, E. MAIRE, P. MERLE and G. PEIX, "X-ray Tomography in Materials Science" (Hermes Science Publications, Paris, 2000).
24. P. FREY, B. SARTER and M. GAUTHERIE, *Int. J. Methods Eng.* **37** (1994) 2735.
25. J. ROUILLE, G. DELLA VALLE, M. F. DEVAUX, D. MARION and L. DUBREIL, *Cereal Chem.* (2004) in press.
26. T. VAN VLIET, A. M. JANSSEN, A. H. BLOKSMA and P. WALSTRA, *J. Texture Studies* **23** (1992) 439.

Received December 2004
and accepted April 2005